A&A 543, A151 (2012)
DOI: 10.1051/0004-6361/201219206
© ESO 2012

Astronomy & Astrophysics

The bipolar outflow and disk of the brown dwarf ISO 217⋆

V. Joergens[1,2], A. Pohl[2], A. Sicilia-Aguilar[3], and Th. Henning[2]

[1] Zentrum für Astronomie Heidelberg, Institut für Theoretische Astrophysik, Albert-Ueberle-Str. 2, 69120 Heidelberg, Germany
e-mail: viki@mpia.de
[2] Max-Planck Institut für Astronomie, Königstuhl 17, 69117 Heidelberg, Germany
[3] Departamento de Física Teórica, Facultad de Ciencias, Universidad Autónoma de Madrid Cantoblanco, 28049 Madrid, Spain

Received 9 March 2012 / Accepted 6 May 2012

ABSTRACT

We show that the very young brown dwarf candidate ISO 217 (M6.25) is driving an intrinsically asymmetric bipolar outflow with a stronger and slightly faster red-shifted component based on spectro-astrometry of forbidden [S II] emission lines at 6716 Å and 6731 Å observed in UVES/VLT spectra taken in 2009. ISO 217 is only one of a handful of brown dwarfs and very low-mass stars (M5–M8) for which an outflow has been detected and that show that the T Tauri phase continues at the substellar limit. We measure a spatial extension of the outflow in [S II] of up to ±190 mas (about ±30 AU) and velocities of up to ±40–50 km s^{-1}. We find that the basic outflow properties (spatial extension, velocities, and outflow position angle) are of similar order as those determined in the discovery spectra from May 2007 of Whelan and coworkers. We show that the velocity asymmetry between both lobes is variable on timescales of a few years and that the strong asymmetry of a factor of two found in 2007 might be smaller than originally anticipated when using a more realistic stellar rest-velocity. We also detect forbidden line emission of [Fe II]λ7155 Å, for which we propose as a potential origin the hot inner regions of the outflow. To comprehensively understand the ISO 217 system, we determine the properties of its accretion disk based on radiative transfer modeling of the SED from 0.66 to 24 μm. This disk model agrees very well with *Herschel*/PACS data at 70 μm. We find that the disk is flared and intermediately inclined ($i \sim 45°$). The total disk mass of the best-fit model is $4 \times 10^{-6}\ M_{\odot}$, which is low compared to the accretion and outflow rate of ISO 217 from the literature ($\sim 10^{-10}\ M_{\odot}$ yr^{-1}). We propose that this discrepancy can be explained by either a higher disk mass than inferred from the model because of strong undetected grain growth and/or by an on average lower accretion rate and outflow rate than the determined values. We show that a disk inclination significantly exceeding 45°, as suggested from Hα modeling and from both lobes of the outflow being visible, is inconsistent with the SED data. Thus, despite its intermediate inclination angle, the disk of this brown dwarf does not appear to obscure the red outflow component in [S II], which is very rarely seen for T Tauri objects (only one other case).

Key words. brown dwarfs – stars: pre-main sequence – circumstellar matter – stars: formation – ISM: jets and outflows – stars: individual: ISO 217

1. Introduction

Jets and outflows are a by-product of accretion in the star formation process (e.g., Ray et al. 2007, for a review). They have been observed for many classical T Tauri stars (CTTS) in terms of the emission in atomic and molecular lines that originates in the radiative cooling zones of shocks with moderate to large velocities (a few tens to a few hundred km s^{-1}). These detections have been made either directly through narrow-band imaging, e.g. in molecular lines of CO or forbidden emission lines (FELs), or through spectro-astrometry of FELs (in some cases also of Hα emission lines). It has been suggested that jets transport a significant amount of excess angular-momentum from the accretion disk, as some jets have been found to rotate (e.g., Launhardt et al. 2009). The observed correlation between mass outflow and disk accretion indicates a magnetohydrodynamic jet-launching mechanism. The jet could originate from either a wide range of disk radii ("disk wind model"), as favored by a high-resolution kinematic and collimation study of [Fe II] emission in DG Tau (Agra-Amboage et al. 2011), or the interface between the star's magnetosphere and the disk ("X wind model"). Typical mass-loss rates for CTTS are found to be on the order of 10^{-9}–$10^{-7}\ M_{\odot}$ yr^{-1}, which is about 5% to 10% of the mass accretion rate through the disk (e.g., Sicilia-Aguilar et al. 2006, 2010; Fang et al. 2009).

The technique of spectro-astrometry plays a major role in probing the innermost region of jets, where the central engine is ($\lesssim$10 AU) and most of the collimation and acceleration occurs ($\lesssim$100 AU), and in detecting jets of very low-mass objects, for which the critical density for FELs occurs very close to the driving source (~10–30 AU). Exploring jets on such small scales in nearby star-forming regions (~150 pc) requires milli-arcsecond (mas) resolution. Spectro-astrometry is a means of recovering spatial information well below the diffraction limit of the largest optical/near-infrared (IR) telescopes by measuring the positional centroid of the emission as a function of wavelength of an unresolved star in slit-spectroscopy. The spatial resolution depends here only on the ability to measure the centroid position. The application of this method to CTTS was developed from pioneering work starting in the eighties (Solf 1984; Solf & Böhm 1993; Hirth et al. 1994a, 1997) to resolve jets at 10 AU from the central source (e.g., Garcia et al. 1999; Takami et al. 2001, 2003) and to discover the jets of brown dwarfs (Whelan et al. 2005).

While many details about the origin of brown dwarfs are still unknown, it has been established in the past few years that brown

⋆ Based on observations obtained at the Very Large Telescope of the European Southern Observatory at Paranal, Chile in program 079.C-0375(A), 080.C-0904(A), and 082.C-0023(A+B).

dwarfs during their early evolution resemble higher mass T Tauri stars in many properties. Very young brown dwarfs (a few Myr) display chromospheric activity, such as surface spots (e.g., Joergens et al. 2003). There is evidence that brown dwarfs have disks from mid-IR (e.g., Comerón et al. 2000; Jayawardhana et al. 2003; Luhman et al. 2008) and far-IR/submm excess emission (Klein et al. 2003; Scholz et al. 2006; Harvey et al. 2012a). Many of these disks have been found to be actively accreting (e.g., Mohanty et al. 2005; Herczeg & Hillenbrand 2008; Bacciotti et al. 2011; Rigliaco et al. 2011) and several show signs of grain growth and crystallization (e.g., Apai et al. 2005; Pascucci et al. 2009). Furthermore, very young brown dwarfs rotate on average much slower (e.g., Joergens & Guenther 2001; Joergens et al. 2003; Caballero et al. 2004) than their older counterparts (e.g., Bailer-Jones & Mundt 2001; Mohanty & Basri 2003), which is indicative of a magnetic braking mechanism due to interaction with the disk.

The first indication that brown dwarfs and very low-mass stars (VLMS) might also be able to drive T Tauri-like outflows came from the observation of forbidden emission in the spectrum of an M6.5 dwarf, which is known to be an active accretor (LS-R CrA 1, Fernandez & Comerón 2001). Spectro-astrometry of detected forbidden [S II], [O I], and [NII] emission of several brown dwarfs and VLMS then provided proof that objects of a tenth of a solar mass to less than 30 $M_{\rm Jup}$ can launch powerful outflows: Par-Lup3-4 (M5), ρ Oph 102 (M5.5[1]), ISO 217 (M6.25), LS-R CrA 1 (M6.5), 2M1207 (M8), and ISO-Oph 32 (M8) (Whelan et al. 2005, 2007, 2009a,b; Bacciotti et al. 2011; cf. also Fernandez & Comerón 2005; Looper et al. 2010). This was further supported by a resolved image of the outflow of the VLMS ρ Oph 102 (M5.5), which was detected in the CO $J = 2{-}1$ transition with a 10 arcsec spatial offset from the central source (Phan-Bao et al. 2008; cf. also Phan-Bao et al. 2011). Directly resolving brown dwarf outflows in FELs is, on the other hand, challenging (e.g., Wang & Henning 2006) because the critical density of FELs occurs at very close separations (of ∼100 mas at a distance of ∼150 pc).

The investigated brown dwarfs and VLMS exhibiting outflows constitute a small sample of six objects, out of which only four have a spectral type later than M6 (ISO 217, LS-R CrA 1, 2M1207, ISO-Oph 32), i.e. are at or below the substellar border. They seem to have similar (scaled-down) properties as CTTS jets in several respects, as for example they can be asymmetric and their FEL regions appear to contain both low and high velocity components. First estimates of their mass-loss rates ($\dot{M}_{\rm out} = 10^{-9}{-}10^{-10}\,M_\odot\,{\rm yr}^{-1}$, Whelan et al. 2009a; Bacciotti et al. 2011) and comparisons with mass accretion rates for brown dwarfs ($\dot{M}_{\rm acc} = 10^{-9}$ and $10^{-11}\,M_\odot\,{\rm yr}^{-1}$, e.g., Muzerolle et al. 2003; Natta et al. 2004; Mohanty et al. 2005; Herczeg & Hillenbrand 2008) give tentative hints of a relatively high $\dot{M}_{\rm out}/\dot{M}_{\rm acc}$ ratio, e.g. 40% for Par-Lup3-4 (Bacciotti et al. 2011). However, given the small number of only a handful of detected outflows for brown dwarfs and VLMS, for most of which only single epoch observations are made, the available data do not yet provide a robust data set to help us establish their properties. Important questions remain, concerning for example the degree of collimation and possible variability.

We explore here the bipolar outflow of the brown dwarf candidate ISO 217 (M6.25) by means of spectro-astrometry of high-resolution UVES/VLT spectra taken two years after the discovery data. In a complementary fashion, we determine the disk properties of ISO 217 based on radiative transfer modeling of its spectral energy distribution (SED) to comprehensively understand the disk and outflow system. The paper is organized as follows: after a summary of the known properties of ISO 217 (Sect. 2), the observations on which our work is based are described (Sect. 3). Section 4 presents the modeling of the disk using flux measurements from the literature. In the next three sections, our high-resolution UVES spectra of ISO 217 are exploited by studying emission line profiles (Sect. 5), performing a spectro-astrometric analysis of forbidden [S II] emission (Sect. 6), and analyzing our spectro-astrometric detection of the bipolar outflow (Sect. 7). Section 8 provides a discussion and conclusion of the ISO 217 disk and outflow system.

2. The brown dwarf candidate ISO 217

ISO 217[2] is an M6.25 type very low-mass object (Muzerolle et al. 2005; Luhman 2007) located in the Chamaeleon I (Cha I) star-forming region at a distance of ∼160–165 pc. An estimate of its mass based on a comparison of effective temperature and luminosity ($T_{\rm eff} = 2962$ K, $L_{\rm bol} = 0.023\,L_\odot$, Luhman 2007) with evolutionary models (Baraffe et al. 1998) yields a value of about 0.08 $M_\odot$, i.e. close to the hydrogen burning limit.

Mid-IR excess emission of ISO 217 was detected by the Infrared Space Observatory Camera (ISOCAM, Persi et al. 2000; Lopez Marti et al. 2004) and the *Spitzer* space mission (Apai et al. 2005; Pascucci et al. 2009; Luhman et al. 2008) showing that ISO 217 has a disk. A strong 10 μm silicate emission detected in a spectrum taken by the *Spitzer*/InfraRed Spectrograph (IRS) gives evidence of both grain growth and moderate crystallization in this disk (Apai et al. 2005). The disk inclination was suggested to be 65° based on modeling of the Hα line profile (Muzerolle et al. 2005; the inclination is defined here as the angle between the line-of-sight and the stellar rotation axis, so that 90° corresponds to an edge-on system, Muzerolle, priv. comm.).

ISO 217 displays broad Hα emission with an equivalent width (EW) varying between 70 Å and 230 Å indicating ongoing variable disk accretion (Muzerolle et al. 2005; Luhman 2004; Scholz & Jayawardhana 2006, this work). Scholz & Jayawardhana (2006) found that the variability of the Hα line can be predominantly attributed to the emission wings and thus to high-velocity infalling gas. Furthermore, a blue-shifted absorption dip present in the Hα profile (Scholz & Jayawardhana 2006; Whelan et al. 2009a) appears to correspond to a wind with a velocity of between a few and about 30 km s^{-1}. An estimate of the accretion rate based on a magnetospheric model of the Hα line profile at one epoch yields $1.0 \times 10^{-10}\,M_\odot\,{\rm yr}^{-1}$ (Muzerolle et al. 2005), which is a typical value for brown dwarfs and VLMS.

The presence of forbidden [S II]λ6731 line emission in some spectra of ISO 217 taken by Scholz & Jayawardhana (2006) gave the first hints for the outflow activity of this very low-mass object. A spectro-astrometric analysis of forbidden line emission in [S II]λ6731, [S II]λ6716, [O I]λ6300, and [O I]λ6363 revealed that ISO 217 is driving a bipolar outflow with an estimated mass-loss rate of $2{-}3 \times 10^{-10}\,M_\odot\,{\rm yr}^{-1}$ (Whelan et al. 2009a). We explore the properties of this bipolar outflow based on spectro-astrometry of [S II]λ6731 and [S II]λ6716 emission recorded two years after the discovery data. Furthermore, we determine the disk properties of ISO 217 by means of SED modeling.

[1] Spectral type ρ Oph 102: Luhman (priv. comm.).

[2] Simbad name: ISO-ChaI 217.

3. Observations

3.1. The spectral energy distribution of ISO 217

To model the disk of ISO 217 (Sect. 4), we used optical to mid-IR flux measurements from the literature. The existing photometry in optical (RI) and near-IR (*JHK*) bands is mainly based on observations by the ESO 2.2 m/Wide Field Imager (Lopez Marti et al. 2004), the Two Micron All Sky Survey, and the Deep Near Infrared Survey of the Southern Sky (e.g., Carpenter et al. 2002). Mid-IR photometry of ISO 217 was obtained by ISOCAM (6.7 μm, Persi et al. 2000; Lopez Marti et al. 2004), the InfraRed Array Camera (IRAC) on board the *Spitzer* satellite (3.6, 4.5, 5.8, 8.0 μm), and the Multiband Imaging Photometer for *Spitzer* (MIPS, 24 μm, Luhman et al. 2008). In addition, a *Spitzer*/IRS spectrum (7.4–14.5 μm) was taken (Apai et al. 2005; Pascucci et al. 2009). Very recently, ISO 217 was observed in the far-IR by the Photoconductor Array Camera and Spectrometer (PACS) of the *Herschel* mission (Harvey et al. 2012b). We show in Sect. 4 that our disk model, which is based on the SED up to 24 μm, is in very good agreement with the *Herschel* flux measurement at 70 μm.

Photometric variability. The star appears to be significantly variable at optical and IR wavelengths (Fig. 1). In particular, the IRS observations indicate that the flux is higher by nearly a factor of two than in the IRAC 8 μm observation. The ISOCAM data, on the other hand, detect a flux that is about 30% fainter than the IRAC data. This strong variability from optical to mid-IR wavelengths suggests that the cause of the variations is an increase in the luminosity of the star (for instance, owing to a higher accretion rate) rather than an occultation effect. On the basis of the observed variability in the 8 μm region, it can be expected that the 24 μm flux is also variable for this object (e.g., Muzerolle et al. 2009). The single-epoch MIPS data were not taken simultaneously with any other photometry, therefore the average 24 μm flux level and the 8–24 μm slope remain somewhat uncertain. This as well as the the mid-IR data not being taken simultaneously with the optical/near-IR data, which represent the (sub)stellar photosphere, complicated the SED modeling (Sect. 4).

3.2. High-resolution spectroscopy of ISO 217

Spectroscopic observations of ISO 217 were obtained within the framework of a high-resolution spectroscopic study of young brown dwarfs and VLMS in Cha I (e.g., Joergens 2006, 2008). ISO 217 was observed for three nights in 2008 and 2009 in the red optical-wavelength regime with the Ultraviolet and Visual Echelle Spectrograph (UVES, Dekker et al. 2000) attached to the VLT 8.2 m KUEYEN telescope. The spectral resolution $\lambda/\Delta\lambda$ was 40 000 and the spatial sampling 0.182″/pixel. An observing log is given in Table 1. We used UVES spectra that were reduced, and both wavelength- and flux-calibrated using the ESO UVES pipeline in order to study activity-related emission lines (Ca II, [S II], [Fe II]) in terms of their line profile shapes and line strengths (Sect. 5). Furthermore, a spectro-astrometric analysis of the detected forbidden line emission in [S II] was performed based on a custom-made reduction and wavelength calibration procedure (Sect. 6).

Stellar rest-velocity. The stellar rest-velocity of ISO 217 was determined based on a Gaussian fit to the Li I doublet lines at 6707.76 Å and 6707.91 Å in the pipeline-reduced spectra. This Li I doublet was not resolved in our observations, therefore, their mean value (6707.84 Å) was adopted as a reference in the velocity measurement. We note that the maximum error possibly introduced by the assumption of two equally strong lines was estimated to be less than 1 km s^{-1} by using a high-resolution synthetic PHOENIX spectrum of similar stellar parameters (Husser et al. 2012). The radial velocities determined in this way and their errors, which are based on the Gaussian fit, are listed in Table 1 for the average spectra of each night. They agree well with the radial velocities measured for other brown dwarfs and T Tauri stars in Cha I (e.g. Covino et al. 1997; Joergens 2006; James et al. 2006). Their weighted mean value $V_0 = (17.2 \pm 1.3)$ km s^{-1} was adopted as stellar rest-velocity for ISO 217, relative to which all velocities in the following are given.

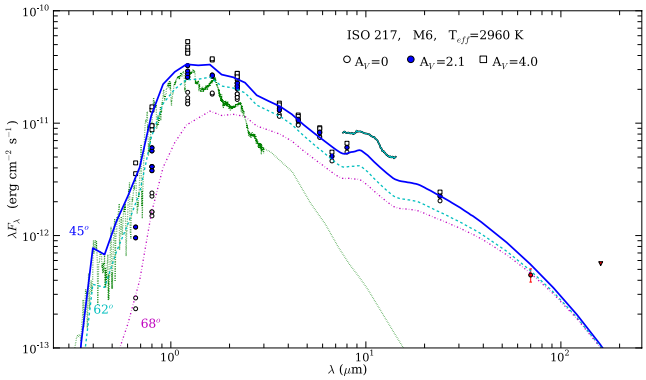

Fig. 1. SED and disk model for ISO 217. Flux measurements are plotted for extinction values of A_v = 0, 2.1, and 4 mag, as denoted. The displayed models are a PHOENIX photosphere model (green dotted line) and our best-fit disk model for an inclination of i = 45° (dark blue line). For comparison, we also show disk models for i = 62° (turquoise dashed line) and 68° (pink dash-dotted line).

4. Modeling the disk of ISO 217

The outflow activity of young stellar objects is intrinsically tied to the accretion disk. To gain a comprehensive understanding of the ISO 217 outflow and disk system, we determined the disk properties (structure, orientation, and mass) of ISO 217 by means of radiative transfer modeling of its SED (Fig. 1). A disk has been detected around ISO 217 based on mid-IR excess emission (cf. Sects. 2 and 3.1), though no SED modeling of this disk has yet been performed. The suggested high inclination-angle of the ISO 217 disk, which was inferred from a modeling of the Hα profile (65°, Muzerolle et al. 2005) and from both lobes of the outflow being visible (Whelan et al. 2009a), requires verification by an SED model.

We fitted the observed SED of ISO 217 from the optical to the mid-IR (0.66–24 μm, cf. Sect. 3.1) with the radiative transfer code RADMC[3] of Dullemond & Dominik (2004). The RADMC package was designed to model three-dimensional (3D) axisymmetric circumstellar-dust configurations, and was tested extensively for continuum radiative transfer in protoplanetary disks. Although assuming axisymmetry reduces the problem to two dimensions, the photon packages are followed in 3D. The code uses a variant of the Monte Carlo method of Bjorkman & Wood (2001) to compute how the stellar photons penetrate the disk and to determine the dust temperature and scattering source function at any location in the disk. Applying volume ray-tracing

[3] See http://www.ita.uni-heidelberg.de/~dullemond/software/radmc/

Table 1. Observing log, slit position angle, and radial velocity of ISO 217.

Name	Date	HJD	Exptime [s]	Seeing [arcsec]	Slit PA [deg]	RV [km s^{-1}]
spec 1	2008 03 22	2 454 547.61149	2 × 1500	0.93	158.9 ± 7.3	
spec 2	2008 03 22	2 454 547.64793	2 × 1500	0.78	173.8 ± 7.4	16.8 ± 2.2
spec 3	2009 01 30	2 454 861.68128	2 × 1500	1.08	131.7 ± 6.9	
spec 4	2009 01 30	2 454 861.71766	2 × 1500	1.10	146.0 ± 7.1	17.4 ± 1.6
spec 5	2009 02 23	2 454 885.70518	2 × 1500	0.79	167.2 ± 7.4	
spec 6	2009 02 23	2 454 885.74161	2 × 1500	0.69	182.3 ± 7.5	17.4 ± 2.4

Notes. The HJD is given at the middle of the exposure; the seeing is the averaged seeing corrected by airmass; the slit position angle (PA) was not kept fixed during observations and each 2 × 1500 s exposure samples a PA range of about ±7 deg, as listed; the radial velocity (RV) is determined based on a fit to the Li I (λ 6708 Å) line in the averaged spectra of each night.

allows us to determine the spectra and images for all inclination angles. The code can be modified by selecting disk mass, flaring, outer radius, vertical height of the disk at the outer radius, and dust grain distribution. In all cases, it is assumed that the dust and gas are well-mixed (i.e. there is no differential settling for grains with different masses) and that all grains have the same temperature distribution.

For the photosphere of the star, we used a PHOENIX model (Hauschildt et al. 1999) with $T_{\rm eff}$ = 2960 K and log(g) = 4.0 (green dotted line in Fig. 1). To reproduce the integrated luminosity, the stellar radius was set to R_* = 0.6 $R_\odot$. Since there is no evidence of an inner disk hole, we located the inner rim of the disk at the dust destruction radius, which for a dust destruction temperature of 1500 K is about 4 R_*. This agrees with the corotation radius (3−9 R_*) that was derived for ISO 217 by considering typical rotational periods of young brown dwarfs and VLMS (1−5 d, Joergens et al. 2003; Rodríguez-Ledesma et al. 2009). The outer disk radius was chosen to be $R_{\rm disk}$ = 100 AU, although it is not well-constrained by any data. The disk mass was varied and then determined by requesting a good fit to the 24 μm data point.

The object was assumed to have a moderate extinction, therefore we considered $A_{\rm V}$ values between 0 mag and 4 mag and a standard extinction law. Different $A_{\rm V}$ values do not have a strong effect on the IR data, but can significantly change the optical fluxes. For our best-fit model (dark blue line in Fig. 1), we adopted the spectroscopically measured extinction of $A_{\rm V}$ = 2.1 mag (converted from A_J = 0.68, Luhman 2007, using the reddening law of Mathis 1990; and R_V = 5.0, Luhman 2004).

The strong variability seen for ISO 217 in the optical to the 8 μm region is a major challenge for SED modeling, in particular given that the data points were not obtained simultaneously (cf. Sect. 3.1). It is indicative of variations in both the accretion rate and luminosity and can be expected to affect also the 24 μm flux (e.g., Muzerolle et al. 2009) and the silicate feature (Abrahám et al. 2009; Juhász et al. 2012). Fortunately, ISO 217 was observed with *Herschel*/PACS at 70 μm (Harvey et al. 2012b), i.e. at wavelengths that play a crucial role in defining the structure and extent of disk material and that are much less affected by variability. We later show that the 70 μm flux measurement strongly supports our approach to the SED fitting. We traced an approximate model focused on the intermediate optical fluxes and the IRAC and MIPS data. Since the IRAC data appear in-between the IRS and ISOCAM observations, we also considered intermediate optical fluxes to estimate the stellar luminosity. We concentrated on reproducing the SED slope between 3 μm and 24 μm and on obtaining a silicate feature similar to the observed one in the IRS spectrum.

The high flux level of ISO 217 in the near-IR suggests that the disk is very flared in its inner regions. The relatively low flux level at 24 μm, on the other hand, could be reproduced by a model that has either a small amount of few-micron-sized grains and/or a low disk flaring and/or a low dust mass. Since the near-IR fluxes indicate a very flared disk and the silicate feature the presence of small grains (e.g., Henning 2010), the low 24 μm flux is most plausibly explained by a low dust mass. We therefore applied a standard flaring law with a pressure scale-height ($H_{\rm p}$) that varies as a power law with the radius, $H_{\rm p}/R \propto R^{1/7}$. The best-fit scale-height at the outer disk radius was found to be $H_{\rm rdisk}/R_{\rm disk}$ = 0.35.

The dusty disk component in the model consists of amorphous Mg-Fe silicates (with Fe and Mg being present in similar proportions; Jäger et al. 1994; Dorschner et al. 1995) and 25% of amorphous carbon grains. While there are signs of crystallization in the disk of ISO 217 from the 10 μm silicate feature (Apai et al. 2005), we found that the energy emitted in crystalline features is negligible compared to that from the continuum plus amorphous features and, thus, that crystallization is not relevant for the SED modeling. We considered a standard dust distribution with grain sizes of between 0.1 μm and 100 μm, that follows a collisional distribution (power law) with an exponent –3.5 (for both silicate and carbon grains alike). Furthermore, a standard gas to dust ratio of 100 was assumed. The best fit was achieved for a model with a total disk mass of $4 \times 10^{-6}\,M_\odot$.

The exploration of different disk orientations yields a best-fit for an intermediate inclination angle i of 45° (dark blue line in Fig. 1). We found that a disk with the described characteristics that has an inclination significantly exceeding 45°, as suggested for example by Hα modeling (65°, Muzerolle et al. 2005), is hard to explain: a disk with an inclination in the range 60°–70° (see Fig. 1 for models with i = 62° and 68°) would not only be inconsistent with the near-IR data, but also produce a much higher extinction than the spectroscopically determined value and compromise the presence of the relatively strong silicate feature. Furthermore, a high extinction would require a flat, settled disk as well as a significantly lower disk mass in order to fit the steep slope at 3–24 μm. A very settled disk, however, is unlikely because high levels of turbulence can be expected given that the object is accreting at a high rate for its low mass and for its low disk mass. Considering that the 24 μm flux might be variable and measured at minimum, only the assumption of a very settled disk would allow for a higher inclination. To summarize, an

inclination angle exceeding 60° is hard to fit within a reasonable disk model.

Our disk model, which is based on flux measurements up to 24 μm, is in very good agreement (within 1.5σ) with recent *Herschel*/PACS observations of ISO 217 at 70 μm (Harvey et al. 2012b), as shown in Fig. 1. This gives us confidence in the disk model developed here because at these longer wavelengths the dependence on the mass and the grain distribution is much stronger, while variability is expected to play a minor role.

The disk mass of ISO 217 derived with our model of $4 \times 10^{-6}\,M_{\odot}$, i.e. about 1 Earth mass, is very low for a CTTS disk but fully consistent with that of other brown dwarfs and VLMS (10^{-5}–$10^{-6}\,M_{\odot}$, e.g., Harvey et al. 2012a). However, it is strikingly low compared to the estimated accretion ($1\times10^{-10}\,M_{\odot}\,\mathrm{yr}^{-1}$, Muzerolle et al. 2005) and mass-loss rate (2–$3\times10^{-10}\,M_{\odot}\,\mathrm{yr}^{-1}$, Whelan et al. 2009a) of ISO 217. Taking these numbers at face value, the total disk mass would be accreted and lost again within less than 40 000 yr, which is unlikely. These discrepancies between dust-inferred disk masses and gas-inferred mass accretion rates are frequently found for CTTS (Hartmann 2008; Sicilia-Aguilar et al. 2011) and are usually explained in terms of a strong grain growth and/or anomalous gas-to-dust ratio. The available SED data for ISO 217 are only sensitive to the presence of small grains because particles with much larger sizes than the longest PACS wavelength do not contribute significantly to the flux owing to their small opacities. Considering a population of large (>100 μm) grains would result in a higher disk mass and might, therefore, account for some of the discrepancy with the gas-inferred mass-accretion rate. However, a disk mass that allows for accretion over a typical disk lifetime of 10^6 yr, would require a hundred times more mass to exist in these large grains. Another possibility is that the accretion rate of ISO 217 was measured in a high state and that it is on average lower than the determined value. This is plausible since this value is based on single epoch observations and since there are several indications of variable accretion of ISO 217 from photometric (Sect. 3.1) and emission-line variability (Scholz & Jayawardhana 2006; Luhman 2007). In this case, there would still remain a mismatch with the outflow rate, which might be a hint that it is also on average lower than the determined value.

The disk around ISO 217 appears at first glance to be in a rather early evolutionary phase given its flared geometry, however, the possibility of undetected strong grain-growth might hint at a more advanced evolutionary stage. ISO 217's disk is consistent with a flared, CTTS-like disk, in agreement with models for many other brown dwarf and VLMS disks (e.g., Natta & Testi 2001; Allers et al. 2006). Several flattened and evolved disks have been identified around objects with similar masses (e.g. Pascucci et al. 2003; Morrow et al. 2008), and are usually traced to more evolved systems with strong settling and grain growth. From this point of view, the disk around ISO 217 could be interpreted as a system that has suffered little evolution. On the other hand, given the possibility of undetected large grains, as described in the previous paragraph, ISO 217 is a good candidate for strong grain growth, despite the flared and primordial appearance of its disk.

5. Observed emission lines of ISO 217

Our UVES spectra of ISO 217 show several emission lines, which are indicative of ongoing accretion, winds, and/or outflowing material (Ca II, [S II], [Fe II]). We studied their line profile shapes and measured their EWs. For this purpose, we used the UVES spectra (Table 1) after reduction, wavelength and flux calibration by the ESO UVES pipeline. Furthermore, the spectral regions of the emission lines were normalized by dividing by a polynomial fit to the continuum emission adjacent to each line. Line profile variations were found to be negligible within one observational night in most cases, allowing us to average spectra from the same night to increase the signal-to-noise ratio (S/R). There was one exception from this, namely the Ca II line profile in the third night (Feb. 23, 2009), which changed significantly on timescales of hours (Fig. 2) and was, therefore, analyzed in the individual spectra. Table 2 lists all observed emission lines, their peak wavelength λ, peak radial velocities v, and the measured EW. The error in the EW is assumed to be 5% of the determined value. The peak values (λ, v) were determined by fitting the line profiles with Gaussian functions and their errors were based on the errors in the fit parameters. In the case of the two lobes of the [S II] lines as well as the [Fe II] line, these errors were underestimated because of deviations from a Gaussian shape. A detailed description of the results for each emission line is provided in the following.

Ca II IR emission. ISO 217 has a broad, asymmetric and variable Ca II IR emission line at 8498 Å (Fig. 2), which implies that this line originates not purely in the chromosphere but also from accretion and/or winds. We note that the other two lines of this IR triplet are not covered by the observations because of a gap in wavelength between the chips of the two-armed spectrograph. The asymmetric Ca II profile displays a red-shifted large velocity tail with velocities of up to 130 km s^{-1}, which could be caused by infalling material. The shape, the peak flux, and the peak velocity of this line vary significantly for spectra taken at different epochs. The line profile shape observed in the third night (Feb. 23, 2009; green and blue profiles in Fig. 2) changed remarkably on timescales of hours. The EW of this line do not generally follow these variabilities; we measured a relatively constant value of about –6 Å apart from the second night (Jan. 30, 2009), where it was –2 Å.

Forbidden [S II] emission. ISO 217 has strong FELs of sulfur [S II] at 6716 Å and 6731 Å (Figs. 5, 6) indicating an origin in a low density region. We measured an EW of about –2 Å to –3 Å for [S II]λ6716 and of about –4 Å to –5 Å for [S II]λ6731, respectively (Table 2). It was shown by Whelan et al. (2009a) and confirmed here (Sect. 7) that these [S II] lines are produced in a bipolar outflow. Both [S II] lines consist of two components, a blue-shifted one with an average peak velocity of –19 km s^{-1} and a red-shifted one with an average peak velocity of 34 km s^{-1} (Table 2). The red component displays a sharp decline at its high velocity edge (between 40 km s^{-1} and 50 km s^{-1}), which is a typical outflow signature. The observed maximum radial velocities of the blue lobe of [S II] range from about –30 km s^{-1} to about –50 km s^{-1}, though they are more difficult to estimate because of the weakness of this line wing. Thus, we observed a velocity asymmetry in the peak emission with the red-shifted component being faster, but this asymmetry is not so obvious in the maximum velocities of these lines (cf. also Sect. 7). It is noticeable that both outflow lobes of ISO 217 are visible and that the red-shifted one is much stronger than the blue-shifted one. This is uncommon for outflows of young stellar objects, because the circumstellar accretion disk usually obscures part of the red-shifted outflowing material. To the best of our knowledge, this has only been observed for one other CTTS (RW Aur, Hirth et al. 1994b). The stronger red-shifted lobe that we see for the [S II] line of ISO 217 hints at an intrinsic asymmetry of the

Table 2. Observed emission lines of ISO 217.

	Date	Lobe	Peak λ [Å]	Peak v [km s^{-1}]	EW [Å]
Ca II	2008 03 22		8498.45 ± 0.02	8.4 ± 1.4	–6.2 ± 0.3
(8498.02 Å)	2009 01 30		8498.22 ± 0.03	1.8 ± 1.5	–2.0 ± 0.1
	2009 02 23 (spec 5)		8498.39 ± 0.02	8.1 ± 1.3	–6.1 ± 0.3
	2009 02 23 (spec 6)		8499.01 ± 0.02	29.8 ± 1.4	–6.3 ± 0.3
	2009 02 23 (spec5&6)		8498.63 ± 0.02	16.4 ± 1.4	–6.2 ± 0.3
[S II]	2008 03 22	red	6731.75 ± 0.01	34.2 ± 1.2	–4.5 ± 0.2
(6730.82 Å)	2008 03 22	blue	6730.46 ± 0.01	–23.0 ± 1.2	
	2009 01 30	red	6731.69 ± 0.01	33.6 ± 1.2	–5.3 ± 0.3
	2009 01 30	blue	6730.36 ± 0.01	–25.7 ± 1.2	
	2009 02 23	red	6731.71 ± 0.01	34.8 ± 1.2	–4.3 ± 0.2
	2009 02 23	blue	6730.54 ± 0.01	–17.4 ± 1.2	
[S II]	2008 03 22	red	6717.35 ± 0.01	33.4 ± 1.2	–2.5 ± 0.1
(6716.44 Å)	2008 03 22	blue	6716.28 ± 0.02	–14.1 ± 1.4	
	2009 01 30	red	6717.33 ± 0.01	34.4 ± 1.2	–3.4 ± 0.2
	2009 01 30	blue	6716.17 ± 0.02	–17.5 ± 1.4	
	2009 02 23	red	6717.34 ± 0.01	35.0 ± 1.2	–2.4 ± 0.1
	2009 02 23	blue	6716.16 ± 0.01	–17.6 ± 1.2	
[Fe II]	2009 02 23		7155.21 ± 0.05	–2.89 ± 2.1	–1.6 ± 0.1
(7155.16 Å)					

Notes. The laboratory wavelengths of the emission lines are taken from the NIST database (http://physics.nist.gov/asd3, Ralchenko et al. 2011). The error in the EW is assumed to be 5% of the determined value. The errors in the peak values (λ, v) are based on the errors in the Gaussian fit parameters. The errors in λ and v are underestimated in the case of deviations from a Gaussian shape ([S II], [Fe II]). See the text for more details.

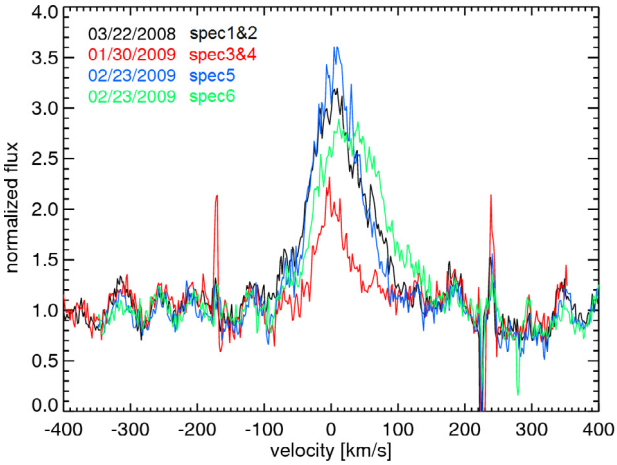

Fig. 2. Ca IIλ8498 emission line in UVES spectra of ISO 217 at different observing times in 2008 and 2009. All fluxes have been normalized to the continuum.

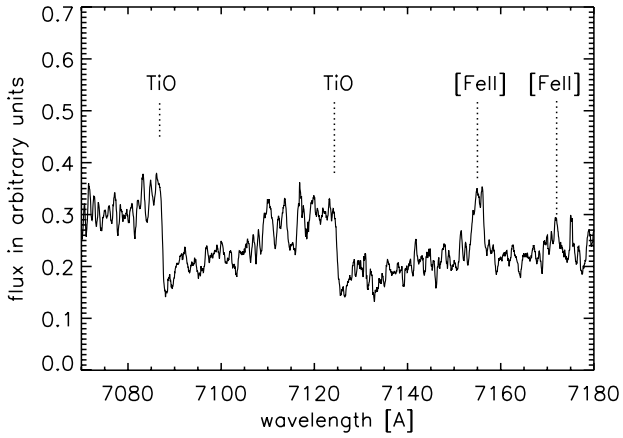

Fig. 3. [Fe II] lines at 7155 Å and at 7172 Å in a mean UVES spectrum of ISO 217. Also displayed are two TiO absorption band-heads at 7087 Å and 7124 Å for comparison.

outflow of ISO 217 and at no or only little obscuration by the disk.

Forbidden [Fe II] emission. ISO 217 displays forbidden line emission in [Fe II] at 7155 Å (Fig. 3). The measured EW is 1.6 Å and the line is emitted at relatively small blue-shifted velocities (–3 km s^{-1} at line peak). Furthermore, there is tentative evidence of [Fe II] emission at 7172 Å. Emission in [Fe II] has also been observed for jets of T Tauri stars (e.g., Hartigan et al. 2004). We note that the [Fe II] line at 8617 Å is not covered by our observations (because of a gap between CCD chips), which prevents us from measuring the electron density in the densest regions of the outflow based on the [Fe II] λ7155/λ8617 ratio (cf. Hartigan et al. 2004). Interestingly, we observe the [Fe II]λ7155 Å emission of ISO 217 solely from the blue-shifted component and at significantly smaller velocities than the [S II] emission. In the following, we show that the [Fe II] emission could originate from regions of higher temperatures than [S II]: the ratio of the [S II] lines λ6716/λ6731 strongly depends on the electron density and temperature. Considering the values observed for ISO 217 (about 0.6, cf. Table 2), we derived electron densities of about 1–3 × 10^3 cm^{-3} for temperatures between 1000 K and 10 000 K (Osterbrock 1989, p. 422). When restricting the temperature range to more reasonable values for a brown dwarf environment of 1000–3000 K, we found a density range of 1–2 × 10^3 cm^{-3}. On the other hand, the [Fe II] line ratio λ7155/λ7172 is much more sensitive to temperature than to electron density; for the considered density range it is practicably

independent of the density. We roughly estimated the observed [Fe II] λ7155/λ7172 line ratio of ISO 217 to about 4, which corresponds to a temperature in the range 2000–5000 K (NIST database, Ralchenko et al. 2011). Therefore, the differences observed between the [S II] and [Fe II] lines could indicate that the [Fe II] emission is produced in a hotter environment. A possible scenario is then that the [Fe II] emission originates from the hot (and dense), inner regions of the outflow, where the bulk of the acceleration has not yet taken place, and where occultation by the disk occurs more easily than at greater radii.

Hα emission. In addition to our own data, we also measured EWs for the Hα line in spectra from May 2007 taken by Whelan et al. (2009a). The EW of Hα determined from these (pipeline-reduced and flux-calibrated) spectra is -137 ± 7 Å, which is consistent with previous Hα EW measurements for ISO 217 (-137 ± 7 Å, Luhman 2004; between –70 Å and –230 Å, Muzerolle et al. 2005; Scholz & Jayawardhana 2006).

6. Spectro-astrometric analysis

We performed a spectro-astrometric analysis of the detected forbidden line emission of [S II] in the two-dimensional (2D) spectra of ISO 217. After completing a standard CCD reduction of the raw data (bias and flatfield correction and cosmic-ray elimination), a row-by-row wavelength calibration of the 2D spectra of individual echelle orders was done using the longslit package (fitcoords/transform) of IRAF. Finally, the sky was subtracted. We note that the detected spectro-astrometric signatures of [S II] are even visible in the unprocessed data, which demonstrates that the data reduction procedure does not introduce any artificial spatial offsets.

We measured the spectro-astrometric signature in the resulting 2D spectra by Gaussian fitting the spatial profile at each wavelength of both the FELs and the adjacent continuum, following e.g. Hirth et al. (1994a). The spatial offset in the FEL was then computed relative to the continuum. In detail, the spatial position y_C of the central source was first determined by Gaussian fitting the continuum emission in the spatial direction using spectral regions free of FELs. Secondly, the continuum emission was removed by fitting the continuum on either side of the FEL row by row with a low-order polynomial and subtracting these fits (cf. e.g., Davis et al. 2003). This continuum subtraction plays an important role in revealing the weak FELs, as demonstrated e.g. by Hirth et al. (1994a). Finally, the spatial centroid position of the FEL y' was measured in the continuum-subtracted spectrograms and the spatial offset $y = y' - y_C$ is computed as a function of the wavelength/velocity. Velocities are given relative to the stellar rest-velocity of ISO 217, as determined in Sect. 3.2.

A challenging aspect of the application of spectro-astrometry to high-resolution spectra of brown dwarfs and VLMS is the faintness of the emission lines. For the described spectro-astrometric analysis, the data were binned in the wavelength direction in order to increase the S/R, as commonly done in the spectro-astrometry of brown dwarfs (e.g., Whelan et al. 2009a). During the Gaussian fit procedure, the best-fit was found and its quality assessed by using the χ^2-method. In cases where the fit did not sufficiently represent the observed spectrum, these continuum data points were excluded from the plot. It was found that the spectra taken in Feb. 2009 have the highest S/R and are best-suited for a spectro-astrometric analysis, whereas the poorer quality of the spectra from Mar. 2008 and Jan. 2009 prevent us from performing a quantitative spectro-astrometry of these data.

The UVES observations were originally optimized for radial velocity work, therefore, the slit orientation was kept aligned with the direction of the atmospheric dispersion. As a consequence, the slit position angle (PA) changed relative to the sky during the observations: each 2×1500 s exposure samples a range of on-sky PAs of about ±7°, as given in Table 1. The mean slit PA of the spectra are between 130° and 180°. While a varying slit PA is not ideal for spectro-astrometry, for which one would like to keep the slit PA constant during an exposure, the data allow nevertheless the detection of outflows of our target.

To rule out spectro-astrometric artefacts, which can be caused for example by an asymmetric PSF (Brannigan et al. 2006), we applied spectro-astrometry to a photospheric absorption line (KI λ7699) and demonstrated that it has no spectro-astrometric signature (spatial offset smaller than 50 mas, see Fig. 4).

7. Results of spectro-astrometry

We have clearly detected the spectro-astrometric signature of a bipolar outflow in both [S II] lines in our UVES spectra of ISO 217. For the quantitative spectro-astrometric analysis, we focused on the spectra taken in Feb. 2009 because they have the highest S/R. Figures 5, 6 show in the top panels the line profiles of both the [S II]$\lambda\lambda$6716, 6731 lines in these spectra and in the bottom panels the measured spatial offsets of both the continuum and the FEL as a function of velocity. The plotted errors in the spectro-astrometric plots are based on 1σ errors in the Gaussian fit parameters. Table 3 lists the maximum spatial offsets and corresponding velocities for both the blue and the red components of both [S II] lines. These maximum spatial offsets were estimated from the weighted average of the two points with the largest offsets, to ensure that our measurement was less sensitive to outliers. Offset errors in Table 3 are based on the standard deviation in the continuum points. For an overview and to constrain the outflow PA (see below), we plot the maximum spatial offsets in Fig. 7 as a function of the slit PA.

Our spectro-astrometric analysis of the detected FELs of [S II] demonstrated that they originate from spatially offset positions on either side of the continuum source of up to ±190 mas (about ±30 AU at the distance of Cha I) at a velocity of up to ±40–50 km s^{-1}.

We found the [S II]λ6716 emission to be spatially more extended than the [S II]λ6731 emission in all but one case (Table 3, Fig. 7), which is consistent with the [S II]λ6716 line tracing lower densities than the [S II]λ6731 line.

The asymmetry seen for the two lobes in the [S II] line profiles, where the red lobe is much stronger and also faster (top panels in Figs. 5, 6, Sect. 5), is a remarkable feature of the ISO 217 outflow. In accordance with this, we observed in the spectro-astrometry of these lines a tendency for the blue lobe to be slower and more extended: (i) the measured outflow velocities range between –30 km s^{-1} and –50 km s^{-1} for the blue lobe, and are about 50 km s^{-1} for the red lobe (Table 3); (ii) the spatial offsets measured for the blue lobe are larger than those for the red lobe in all but one case (Table 3, Fig. 7). The exception is the [S II]λ6716 line of spec 6, for which the offset measurement might be affected by an outlying data point (Fig. 5).

The spectra were taken at mean slit PAs of 167° ± 7° and 182° ± 8° (cf. Sect. 6), i.e. not very far from the value determined for the outflow PA of ISO 217 from the 2007 observations of Whelan et al. (2009a, 193–200° for [S II]$\lambda\lambda$6716, 6731). As illustrated in Fig. 7, we found for an increasing mean slit PA from 167° to 182°, either a slight decrease ([S II]λ6716 line) in or a

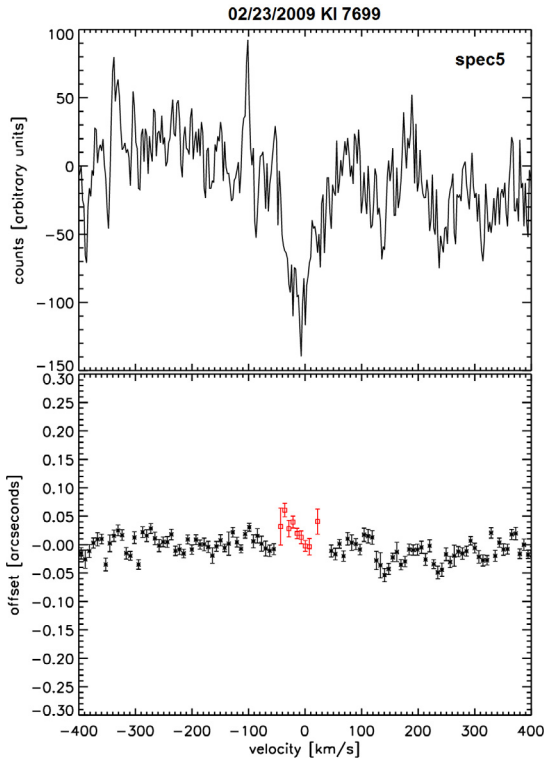

Fig. 4. Spectro-astrometric analysis of photospheric line KIλ7699 as a test for artifacts. Otherwise same as Fig. 5.

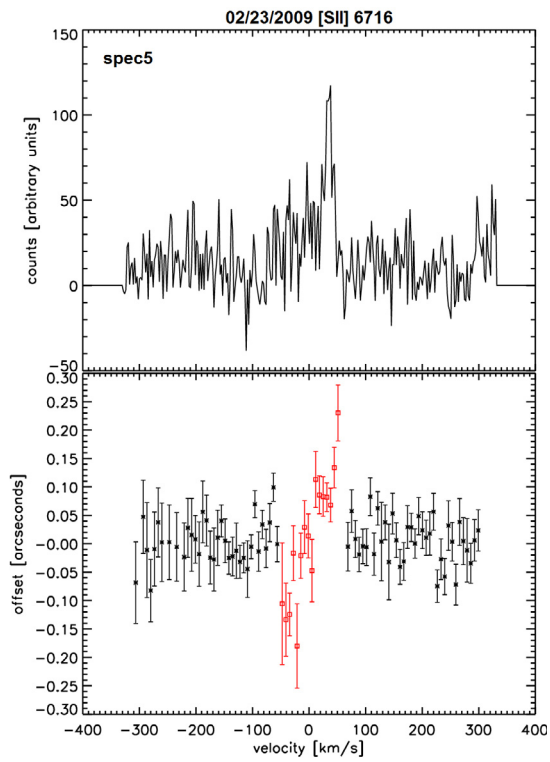

Fig. 5. Spectro-astrometric analysis of the [S II]λ6716 line of ISO 217. *Top panels*: line profiles. Average of 8 pixel rows in the spatial direction centered on the continuum. The continuum has been subtracted. *Bottom panels*: spatial offset vs. radial velocity of the continuum (black asterisks) and of the continuum subtracted FEL (red squares).

constant level ([S II]λ6731) of the observed spatial extension of the outflow. Hence, the data are consistent with an outflow angle that is closer to 170° than 180°. However, the projection of a homogenous outflow with an angle of 200° and an extension of 190 mas onto a slit with a PA of 167° would decrease the observable extension by ~30 mas, which is on the order of the precision of the spectro-astrometry (30–40 mas) performed both here and by Whelan et al. (2009a). The measurement of a different outflow angle for a slightly different slit PA could also be explained by an outflow that has a wide opening angle, causing an almost constant spatial offset for a large range of PAs and/or by an outflow that has a common knot structure (e.g., Hirth et al. 1994b) and for which the measured spatial offset depends on

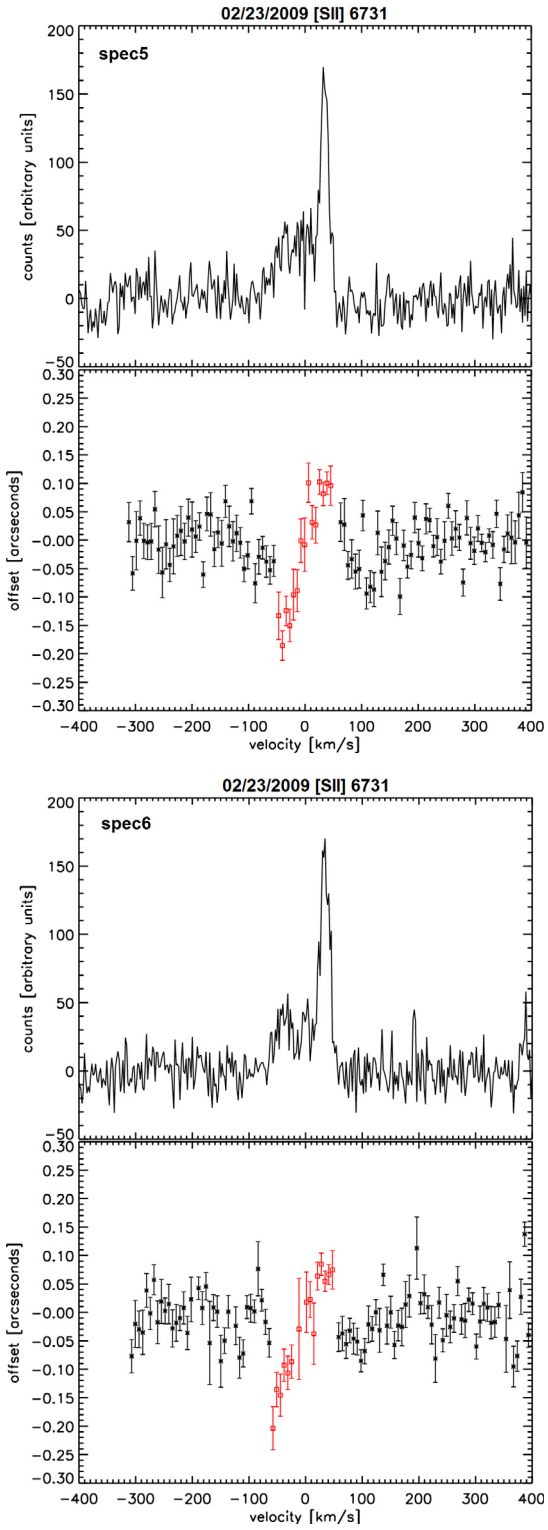

Fig. 6. Spectro-astrometric analysis of the [S II]λ6731 line of ISO 217. Otherwise same as Fig. 5.

whether a knot is detected for a certain slit PA or for example an outside edge of such a knot.

8. Discussion and conclusions

We have proven that the very young brown dwarf candidate ISO 217 (M6.25) is driving a bipolar outflow with a stronger and faster red-shifted component based on spectro-astrometry of [S II] lines in UVES/VLT spectra taken in 2009. ISO 217 is only one of a handful of brown dwarfs and VLMS (M5–M8) for which an outflow has been detected. We have demonstrated that the forbidden [S II] emission in ISO 217 originates from spatially offset positions straddling the central source by up to ±190 mas (about ±30 AU at the distance of Cha I) at a velocity of up to ±40–50 km s^{-1}. There is also evidence of forbidden [Fe II] emission of the blue-shifted component of this outflow. Given the excitation potential of this line, its relatively small velocity (−3 km s^{-1}), and the observation of solely the blue component, we propose as a potential origin of the [Fe II] emission the dense innermost regions, where the outflow has not yet been accelerated.

Table 3. FELs of ISO 217.

Slit PA [deg]	Line	V [km s^{-1}]	Offset (mas)
167.2 ± 7.4	[S II]λ6716	–41 / 48	–197 / 190 (±42)
(spec 5)	[S II]λ6731	–40 / 45	–167 / 102 (±31)
182.3 ± 7.5	[S II]λ6716	–28 / 48	–82 / 146 (±37)
(spec 6)	[S II]λ6731	–54 / 47	–175 / 78 (±30)

Notes. Given are the spatial offsets in milli-arcsec measured by spectro-astrometry and the corresponding radial velocities.

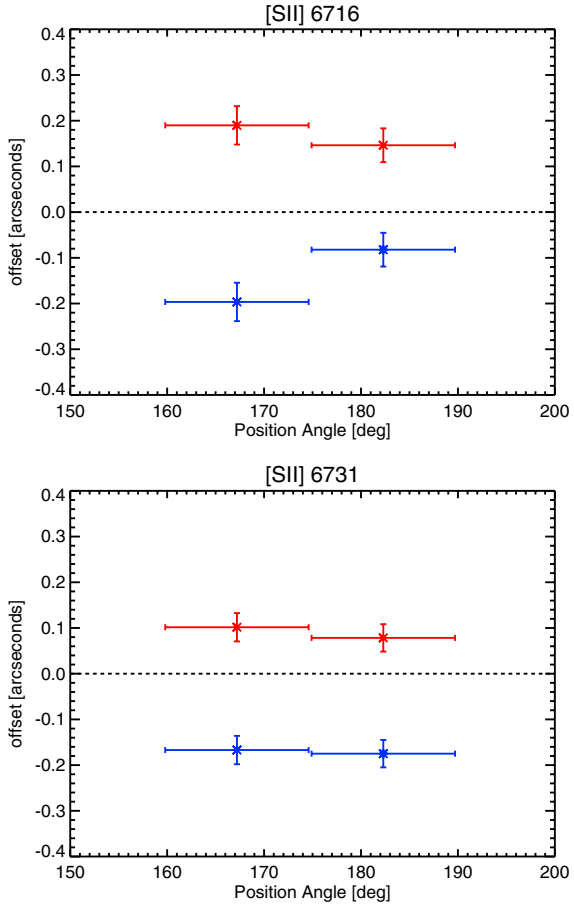

Fig. 7. Spatial offsets of FELs of ISO 217 as a function of the slit PA for [S II]λ6716 (*top panel*) and [S II]λ6731 (*bottom panel*).

We have detected a velocity asymmetry between the two outflow lobes. This can be seen in the [S II] line profiles, where the blue-shifted component has an average peak velocity of –19 km s^{-1} and the red-shifted one of 34 km s^{-1}. Furthermore, the outflow velocities measured using spectro-astrometry tend to be smaller for the blue lobe (between –30 km s^{-1} and –50 km s^{-1}) than for the red lobe (about 50 km s^{-1}). There is tentative evidence that the two lobes are also spatially asymmetric, with the blue component being more extended.

Intrinsic changes in an outflow can occur on timescales of its travel time, which is shorter than three years for ISO 217 given the observed outflow velocity and spatial extension. We have investigated the possible differences of the outflow properties that have been inferred here based on spectra from Feb. 2009 and those determined in the discovery spectra from May 2007 (Whelan et al. 2009a). This is described in detail in the next few paragraphs. Our main results are that we have found that the basic features of the ISO 217 outflow (spatial extension, velocities, and outflow PA) are of similar order in 2007 and 2009, and that the velocity asymmetry between both lobes seem to have decreased slightly in this time period. In addition, we have demonstrated that the strong velocity asymmetry between both lobes of a factor of two found in 2007 might be smaller than originally anticipated when using a more realistic stellar rest-velocity.

The detailed comparison of the outflow properties in 2007 to those in 2009 is described in the following. The line profiles of both [S II] lines have a very similar shape from 2007 to 2009. The noteable differences in the line profiles are slightly less asymmetric peak velocities in 2009 (the difference between blue and red peak of [S II]λ6731 in Feb. 2009 is 17 km s^{-1} compared to 24 km s^{-1} in 2007 at PA = 0°) and a slight decrease in the line strength (the EW of [S II]λ6731 is –4 Å in 2009 compared to –6 Å in 2007). Furthermore, the peak velocities of the [S II] lines (both lobes) appear to be generally shifted by a few km s^{-1} towards the blue from 2007 to 2008/2009. This implies that the velocity of the outflow varied during this time period. We note that the velocities considered in this comparison of the peak velocities were consistently measured using the same stellar rest-velocity of V_0 = 17.2 km s^{-1}, which was derived here for the 2008/2009 spectra.

The spatial extension of the outflow measured by spectro-astrometry in the [S II] lines in 2009 (80–200 ± 35 mas) at slit position angles of 167° ± 7° and 182° ± 8° is to a large degree consistent with that measured in 2007 (180 ± 34 mas) at a slit position angle of 0° (corresponding to 180°, Whelan et al. 2009a). In addition, the observed outflow velocities are of similar order, although, we have found that they are less asymmetric than in 2007: in 2009, the velocity at the maximum spatial offset is about 50 km s^{-1} for the red lobe and between –30 km s^{-1} and –50 km s^{-1} for the blue lobe. The velocities measured by Whelan et al. (2009a) for the 2007 spectra, however, seem to be more asymmetric, with the red-shifted component (40 km s^{-1}) having a velocity approximately twice as large as the blue-shifted one (–20 km s^{-1}). This might be attributed partly to the use of a potentially inaccurate stellar rest-velocity: Whelan et al. (2009a) adopt a stellar rest-velocity of 12.6 km s^{-1}, which is an estimated mean value for T Tauri stars in Cha I. However, this is almost 5 km s^{-1} smaller than the stellar rest-velocity we determined here for and applied to ISO 217 in 2008/2009.

We found that for an increasing slit PA from 167° to 182°, the observed spatial extension of the outflow for both lobes in both [S II] lines either slightly decreases or remains at a constant level. Hence, our data imply that the outflow angle is closer to 170° than 180°, i.e. that it is slightly smaller than but within the errors still consistent with the value measured based on two orthogonal spectra (193–200° in the [S II] lines) by Whelan et al. (2009a).

The outflow activity of young stellar objects is intrinsically tied to the accretion disk. To gain a comprehensive understanding of the ISO 217 outflow and disk system, we have determined the disk properties of ISO 217 by performing a radiative transfer modeling of its SED. The accretion disk surrounding ISO 217 has a total mass of 4×10^{-6} $M_\odot$, a flared geometry, and is viewed under an inclination angle of about 45° according to our model that most accurately fits the observed SED from 0.66–24 μm and that is also in very good agreement with *Herschel*/PACS observations at 70 μm (Harvey et al. 2012b). We have shown that a disk inclination significantly exceeding 45°, as previously suggested based on Hα modeling (65°, Muzerolle et al. 2005) and the visibility of both lobes of the outflow (Whelan et al. 2009a), is inconsistent with the SED data. The disk mass of only about one Earth mass is very low for a CTTS disk, but fully consistent with that of other brown dwarfs and VLMS (10^{-5}–10^{-6} $M_\odot$, e.g., Harvey et al. 2012a). However, it is strikingly low compared to the estimated accretion (1×10^{-10} $M_\odot$ yr^{-1}, Muzerolle et al. 2005) and mass-loss rate (2–3 $\times 10^{-10}$ $M_\odot$ yr^{-1}, Whelan et al. 2009a) of ISO 217. Possible explanations for this discrepancy between the dust-inferred disk mass and the gas-inferred accretion and outflow mass rates are one or both of the following: (i) the disk mass is higher than derived from the model because of a population of large particles (>100 μm) that remain undetected in the available SED data (≤70 μm); (ii) the mass accretion and outflow rates are on average lower than the determined values, which is plausible in the case of the accretion rate given the signs of variable accretion of ISO 217. In the case of undetected strong grain growth, the disk could also be in a more evolved phase than inferred from its flared appearance.

Apart from accretion through the disk and a bipolar outflow, there is also evidence of material falling onto ISO 217 at velocities of up to 130 km s^{-1} (from Ca II IR emission with a red-shifted large-velocity tail, this work) and of a wind expanding at a velocity of up to 30 km s^{-1} (Scholz & Jayawardhana 2006; Whelan et al. 2009a).

To summarize, ISO 217 is a very young M6.25 type object at the substellar limit, that is surrounded by a flared, intermediately inclined accretion disk with possibly strong grain growth. It is driving a bipolar outflow detected in FELs of [S II] with a ±30 AU spatial extension and velocities of up to ±40–50 km s^{-1}. The outflow is intrinsically asymmetric with a stronger and slightly faster red-shifted component. We have found this velocity asymmetry to be variable on timescales of the outflow travel time. The predominance of the red outflow component detected in ISO 217 is very rarely seen for CTTS (only one other case is known, Hirth et al. 1994b) and it implies that the disk does not appear to obscure the red-shifted outflow lobe despite its intermediate inclination angle.

Acknowledgements. We would like to acknowledge the excellent work of the ESO staff at Paranal, who took the data analyzed here in service mode. We thank E. Whelan for valuable discussions on spectro-astrometric analysis and for providing UVES spectra from her program. We also thank P. Harvey, F. Menard, S. Wolf and the rest of the *Herschel* low-mass disk team for providing the PACS flux data for ISO 217 prior to publications. We are grateful for very helpful comments from the referee, T. Ray, which allowed us to improve the paper. Furthermore, we thank I. Pascucci, R. Mundt, R. van Boekel, and C. Dullemond for interesting discussions on varies topics of this paper, as well as R. Smiljanic from the ESO USD for information on position angles. Part of this work was funded by the ESF in Baden-Württemberg. A.S.A. acknowledges support by the Spanish "Ramón y Cajal" program.

References

Ábrahám, P., Juhász, A., Dullemond, C. P., et al. 2009, Nature, 459, 224
Agra-Amboage V., Dougados C., Cabrit S., & Reunanen J. 2011, A&A, 532, A59
Apai, D., Pascucci, I., Bouwman, J., et al. 2005, Science, 310, 834
Bacciotti, F., Whelan, E. T., Alcalá, J. M., et al. 2011, ApJ, 737, L26
Bailer-Jones, C. A. L., & Mundt, R. 2001, A&A, 367, 218
Baraffe, I., Chabrier, G., Allard, F., & Hauschildt, P. H. 1998, A&A, 337, 403
Bjorkman, J. E., & Wood, K. 2001, ApJ, 554, 615
Brannigan, E., Takami, M., Chrysostomou, A., & Bailey, J. 2006, MNRAS, 367, 315
Caballero, J. A., Béjar, V. J. S., Rebolo, R., & Zapatero Osorio, M. R. 2004, A&A, 424, 857
Carpenter, J. M., Hillenbrand, L. A., Skutskie, M. F., & Meyer, M. R. 2002, AJ, 124, 1001
Comerón, F., Neuhäuser, R., & Kaas, A. A. 2000, A&A, 359, 269
Covino, E., Alcalá, J. M., Allain, S., et al. 1997, A&A, 328, 187
Davis, C. J., Whelan, E., Ray, T. P., & Chrysostomou, A. 2003, A&A, 397, 693
Dekker, H., D'Odorico, S., Kaufer, A., Delabre, B., & Kotzlowski, H. 2000, in SPIE 4008, eds. M. Iye, & A. Moorwood, 534
Dorschner, J., Begemann, B., Henning, T., Jaeger, C., & Mutschke, H. 1995, A&A, 300, 503
Dullemond, C. P., & Dominik, C. 2004, A&A, 417, 159
Fang, M., van Boekel, R., Wang, W., et al. 2009, A&A, 504, 461
Fernández, M., & Comerón, F. 2001, A&A, 380, 264
Fernández, M., & Comerón, F. 2005, A&A, 440, 1119
Garcia, P. J. V., Thiébaut, E., & Bacon, R. 1999, A&A, 346, 892
Hartigan, P., Edwards, S., & Pierson, R. 2004, ApJ, 609, 261
Hartmann, L. 2008, Phys. Scr., 130, 014012
Harvey, P. M., Henning, Th., Ménard, F., et al. 2012a, ApJ, 744, L1
Harvey, P. M., Henning, Th., Ménard, F., et al. 2012b, ApJ, accepted
Hauschildt, P. H., Allard, F., & Baron, E. 1999, ApJ, 512, 377
Henning, Th. 2010, ARA&A, 48, 21
Herczeg, G. J., & Hillenbrand, L. A. 2008, ApJ, 681, 594
Hirth, G. A., Mundt, R., & Solf, J. 1994a, A&A, 285, 929
Hirth, G. A., Mundt, R., Solf, J., & Ray, T. P. 1994b, ApJ, 427, L99
Hirth, G. A., Mundt, R., & Solf, J. 1997, A&AS, 126, 437
Husser, T.-O., Hauschildt, P., et al. 2012, submitted
Indebetouw, R., Mathis, J. S., Babler, B. L., et al. 2004, ApJ, 619, 931
Jaeger, C., Mutschke, H., Begemann, B., Dorschner, J., & Henning, Th. 1994, A&A, 292, 641
James, D. J., Melo, C., Santos, N. C., & Bouvier, J. 2006, A&A, 446, 971
Jayawardhana, R., Ardila, D. R., Stelzer, B., & Haisch, Jr. K. E. 2003, AJ, 126, 1515
Joergens, V. 2006, A&A, 448, 655
Joergens, V. 2008, A&A, 492, 545
Joergens, V., & Guenther, E. 2001, A&A, 379, L9
Joergens, V., Fernández, M., Carpenter, J. M., & Neuhäuser, R. 2003, ApJ, 594, 971
Juhász, A., Dullemond, C. P., van Boekel, R., et al. 2012, ApJ, 744, 118
Klein, R., Apai, D., Pascucci, I., Henning, Th., & Waters, L. B. F. M. 2003, ApJ, 593, L57
Launhardt, R., Pavlyuchenkov, Ya, Gueth, F., et al. 2009, A&A, 494, 147
Looper, D. L., Mohanty, S., Bochanski, J. J., et al. 2010, ApJ, 714, 45
López Martí, B., Eislöffel, J., Scholz, A., & Mundt, R. 2004, A&A, 416, 555
Luhman, K. L. 2004, ApJ, 602, 816
Luhman, K. L. 2007, ApJS, 173, 104
Luhman, K. L., Allen, L. E., Allen, P. R., et al. 2008, ApJ, 675, 1375
Mathis, J. S. 1990, ARA&A, 28, 37
Mohanty, S., & Basri, G. 2003, ApJ, 583, 451
Mohanty, S., Jayawardhana, R., & Basri G. 2005, ApJ, 626, 498
Morrow, A. L., Luhman, K. L., Espaillat, C., et al. 2008, ApJ, 676, L143
Mundt, R., & Eislöffel, J. 1998, AJ, 116, 860
Muzerolle, J., Hillenbrand, L., Calvet, N., Briceño, C., & Hartmann, L. 2003, ApJ, 592, 266
Muzerolle, J., Luhman, K. L., Briceñ o, C., Hartmann, L., & Calvet, N. 2005, ApJ, 625, 906
Muzerolle, J., Flaherty, K., & Balog Z. 2009, ApJ, 704, L15
Natta, A., & Testi, L. 2001, A&A, 376, L22
Natta, A., Testi, L., Muzerolle, J., et al. 2004, A&A, 424, 603
Osterbrock, D. E. 1989, Astrophysics of Gaseous Nebulae and Active Galactic Nuclei (Mill Valley, CA: University Science Books)
Pascucci, I., Apai, D., Henning, Th., & Dullemond, C. P. 2003, ApJ, 590, L111
Pascucci, I., Apai, A., Luhman, K., et al. 2009, ApJ, 696, 143
Persi, P., Marenzi, A. R., Olofsson, G., et al. 2000, A&A, 357, 219
Phan-Bao, N., Riaz, B., Lee, C.-F., et al. 2008, ApJ, 689, L141
Phan-Bao, N., Lee, C.-F., Ho, P. T. P., & Tang, Y.-W. 2011, ApJ, 735, 14
Ray, T., Dougados, C., Bacciotti, F., Eislöffel, J., & Chrysostomou, A. 2007, in Protostars and Planets V, eds. B. Reipurth, D. Jewitt, & K. Keil (Tucson: University of Arizona Press), 231
Ralchenko, Yu., Kramida, A. E., Reader, J., & NIST ASD Team 2011, NIST Atomic Spectra Database, http://physics.nist.gov/asd, National Institute of Standards and Technology, Gaithersburg, MD
Rigliaco, E., Natta, A., Randich, S., et al. 2011, A&A, 526, L6
Rodríguez-Ledesma, M. V., Mundt, R., & Eislöffel, J. 2009, A&A, 502, 883
Scholz, A., & Jayawardhana, R. 2006, ApJ, 638, 1056
Scholz, A., Jayawardhana, R., & Wood, K. 2006, ApJ, 645, 1498
Sicilia-Aguilar, A., Hartmann, L. W., Fürész, G., et al. 2006, AJ, 132, 2135
Sicilia-Aguilar, A., Henning, Th., & Hartmann, L. W. 2010, ApJ, 710, 597
Sicilia-Aguilar, A., Henning, Th., Dullemond, C. P., et al. 2011, ApJ, 742, 39
Solf, J. 1984, A&A, 139, 296
Solf, J., & Boehm, K. H. 1993, ApJ, 410 L31
Takami, M., Bailey, J., Gledhill, T. M., Chrysostomou, A., & Hough, J. H. 2001, MNRAS, 323, 177
Takami, M., Bailey, J., & Chrysostomou, A. 2003, A&A, 397, 675
Wang, H., & Henning, Th. 2006, ApJ, 643, 985
Whelan, E. T., Ray, T. P., Bacciotti, F., et al. 2005, Nature, 435, 652
Whelan, E. T., Ray, T. P., Randich, S., et al. 2007, ApJ, 659, L45
Whelan, E. T., Ray, T. P., Podio, L., Bacciotti, F., & Randich, S. 2009a, ApJ, 706, 1054
Whelan, E. T., Ray, T. P., & Bacciotti, F. 2009b, ApJ, 691, L106